Magnetization of a current-carrying superconducting Corbino disk

Ali A. Babaei Brojeny[1,2] and John R. Clem[3]
[1]*Department of Physics, Isfahan University of Technology, Isfahan 84154, Iran*
[2]*International Institute of Theoretical and Applied Physics, Iowa State University, Ames, Iowa 50011-3160*
[3]*Ames Laboratory and Department of Physics and Astronomy, Iowa State University, Ames, Iowa 50011-3160*
(Received 27 March 2001; revised manuscript received 11 July 2001; published 16 October 2001)

We calculate the hysteretic response of a current-carrying type-II superconducting Corbino disk subjected to a perpendicular applied magnetic field. For a disk containing remanent flux in zero field, our theory predicts that applying a radial transport current or raising the temperature at fixed current will cause the magnetic flux to be expelled from the sample. For a disk initially containing no magnetic flux but carrying a radial current, we find that as a perpendicular magnetic field is applied, magnetic-flux penetration occurs in three stages: (i) the magnetic flux gradually penetrates from the edges of the disk until an instability occurs, (ii) there is a rapid inflow of magnetic flux into the disk's central region, which becomes resistive because the radial current density there exceeds the depinning critical current density J_c, and (iii) magnetic flux continues to enter the disk, while persistent azimuthal currents flow in an outer annular region where the net current density is equal to J_c. We also calculate the behavior of a current-carrying Corbino disk subjected to an ac magnetic field.

DOI: 10.1103/PhysRevB.64.184507 PACS number(s): 74.60.Ge, 74.60.Jg, 74.76.−w, 74.60.Ec

I. INTRODUCTION

The properties of a current-carrying type-II superconducting Corbino disk, in which electrical current I fed into the center flows outward through the disk and enters a circumferential electrode at the outer radius R as shown in Fig. 1, are of considerable interest. For example, when the disk is subject to a uniform perpendicular applied magnetic field $\mathbf{B}_a = B_a\hat{z}$ and the resulting vortex array undergoes steady-state flux flow throughout the entire specimen, the resulting electric field $\mathbf{E}=\mathbf{B}\times\mathbf{v}$ has a radial component E_ρ but no azimuthal component. The vortex velocity $\mathbf{v}$ then has only an azimuthal component $v_\phi = -E_\rho/B_z$, and the vortices flow in concentric circular trajectories. Recent experiments by Lopez *et al.*[1,2] in untwinned crystals of $YBa_2Cu_3O_{7-\delta}$ showed that the azimuthal component of the vortex velocity varies as $v_\phi \propto 1/\rho$ in the vortex liquid state, when the Lorentz force causes successive rings of vortices to shear relative to one another as in a liquid, and as $v_\phi \propto \rho$ in the vortex-solid state, when the shear strength of the vortex solid is so strong that the vortex crystal rotates as a whole. However, these authors found that there is a temperature regime of plastic motion in the vortex solid for which v_ϕ has a behavior intermediate between $v_\phi \propto 1/\rho$ and $v_\phi \propto \rho$.

Other experiments in $Bi_2Sr_2CaCu_2O_8$ and 2H-$NbSe_2$ crystals also have revealed that flux flow in the Corbino-disk geometry, where vortices flow in concentric circles, can be quite different from that in the strip geometry, where vortices enter from one side of the sample and exit on the other.[3–6] Rycroft *et al.*[3,4] used both Corbino and strip geometries to show that in the latter case, vortex motion in $Bi_2Sr_2CaCu_2O_8$ crystals can be strongly affected by edge-pinning effects (the Bean-Livingston barrier, the geometrical barrier, or a combination of the two). Eltsev *et al.*[5] used the Corbino-disk geometry to reveal that the vortex-liquid state in $Bi_2Sr_2CaCu_2O_8$ crystals is subdivided into two separate phases with different degrees of transverse vortex correlation. Paltiel *et al.*[6] also used the Corbino geometry to find that the ordered Bragg glass in vortex arrays in 2H-$NbSe_2$ crystals becomes unstable with respect to disorder at both high and low magnetic fields, resulting in a reentrant disorder-driven transition line.

In the present paper, we consider a current-carrying type-II superconducting Corbino disk and calculate its hysteretic response to a perpendicular applied magnetic field. Implicit in this approach is the assumption of a relatively weak vortex-lattice shear strength, such that plastic vortex motion occurs whenever the magnitude of the local Lorentz force density exceeds the maximum pinning force density. The organization of this paper is as follows. In Sec. II, we consider a disk containing remanent flux in zero applied magnetic field and show how the trapped flux is gradually expelled as a radial current is applied. In Sec. III, we consider a zero-field-cooled disk carrying a radial current and show how magnetic flux penetrates into the disk as a perpendicular magnetic field is applied. To treat this problem, in

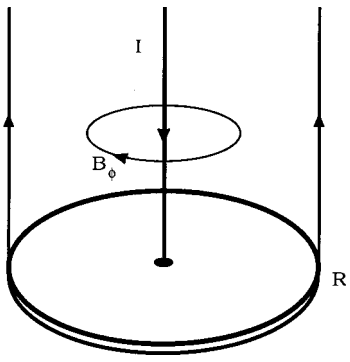

FIG. 1. Sketch of the Corbino disk. Current I flows downward along the center lead, enters the disk at the contact shown, flows outward, and returns upward through a coaxial current return of radius R. This current distribution produces only an azimuthal magnetic field $B_\phi(\rho) = -\mu_0 I/2\pi\rho$ above the disk for radial coordinate $\rho < R$.

which one must account for Meissner screening currents flowing in the inner regions of the disk, we have adopted an integral-equation approach due to Shantsev *et al.*[7,8] We also calculate the magnetization for initial flux penetration. In Sec. IV, we calculate the sequence of current-density and flux-density profiles in a current-carrying Corbino disk when a perpendicular ac magnetic field is applied. We also calculate the corresponding magnetization hysteresis loops. We summarize our results in Sec. V.

II. CURRENT-INDUCED RELAXATION OF TRAPPED FLUX PROFILES STARTING FROM THE REMANENT STATE

Let us consider a thin (thickness $d \ll R$) type-II superconducting disk that has been cooled into the superconducting state in the presence of a large axial applied magnetic field $\mathbf{B}_a = B_a \hat{z}$. We characterize bulk pinning in the superconductor by a magnetic-field-independent critical current density J_c, such that when the applied magnetic field is reduced to zero, a critical-state magnetic-flux distribution, generated by an azimuthal current density (averaged over the thickness of the disk) $\mathbf{J} = J_\phi \hat{\phi}$, where $J_\phi = J_c$, is trapped in the disk. The remanent magnetic field $\mathbf{B}$ can be calculated using the Biot-Savart law. In the plane $z=0$ through the center of the disk, the z component of $\mathbf{B}$ is given to good approximation by[9,10]

$$B_z(\rho,0)/B_d = \frac{1}{\pi J_c}\int_0^R G(\rho,\rho') J_\phi(\rho') d\rho', \tag{1}$$

where

$$G(\rho,\rho') = K[k(\rho,\rho')]/(\rho+\rho') - E[k(\rho,\rho')]/(\rho-\rho'), \tag{2}$$

$$k(\rho,\rho') = 2(\rho\rho')^{1/2}/(\rho+\rho'), \tag{3}$$

K and E are complete elliptic integrals of the first and second kinds, respectively, of modulus k, and $B_d = \mu_0 H_d = \mu_0 J_c d/2$. Here, $H_d = J_c d/2$ is a characteristic flux-penetration field for disk geometry; throughout this paper we shall make use of the corresponding flux density B_d to normalize flux densities.

We next suppose that a current I is fed into the sample as shown in Fig. 1. The average radial current density is

$$J_\rho = I/2\pi\rho d, \tag{4}$$

where ρ is the radial coordinate and d is the thickness of the disk. (The central lead and its contact to the disk have finite radii, thus removing the divergence of J_ρ as $\rho \to 0$.) The current produces a self-field at the top surface of the disk, $B_\phi = -\mu_0 I/2\pi\rho$. Application of the current I upsets the critical-state force balance, because the net current density in the disk is

$$\mathbf{J}(\rho) = J_\phi(\rho)\hat{\phi} + J_\rho(\rho)\hat{\rho}, \tag{5}$$

where J_ϕ depends upon the trapped flux distribution B_z, and J_ρ depends only upon the applied current [Eq. (4)]. The Lorentz force per unit length of vortex is

$$\mathbf{f} = \mathbf{J} \times \phi_0 \hat{z} = (J_\phi \hat{\rho} - J_\rho \hat{\phi})\phi_0, \tag{6}$$

and its magnitude is

$$f = J\phi_0 = (J_\phi^2 + J_\rho^2)^{1/2}\phi_0, \tag{7}$$

where $\phi_0 = h/2e$ is the superconducting flux quantum. Since initially $J_\phi = J_c$, the magnitude of the Lorentz force per unit length f exceeds the maximum pinning force per unit length,

$$f_p = J_c \phi_0, \tag{8}$$

and hence the vortices must move in the direction of the Lorentz force. From Eq. (6), we see that the motion has both an outward radial component and an azimuthal component. While azimuthal vortex motion does not change the magnetic flux density B_z, the radial motion does, and this results in expulsion of magnetic flux from the disk.

We can apply critical-state theory to determine the resulting flux-density profiles B_z. We first note that the resulting vortex distribution depends upon the radial coordinate ρ. Let us define a as the radius at which $J_\rho = J_c$; Eq. (4) yields

$$a = I/2\pi J_c d. \tag{9}$$

For $\rho < a$, the Lorentz force always exceeds the pinning force, the vortices are constantly in motion, and the region $\rho < a$ is resistive. In steady state, for which $d\mathbf{B}/dt = 0$, Faraday's law requires that the azimuthal component of the electric field E_ϕ must be zero. We consider here the case of zero Hall angle, in which $\mathbf{E}$ and $\mathbf{J}$ are parallel, such that we also have

$$J_\phi(\rho) = 0, \quad \rho < a. \tag{10}$$

For $\rho > a$, the final steady-state flux distribution is that for which the magnitude of the Lorentz force per unit length has been reduced to the value of the pinning force per unit length ($f = f_p$). This condition is the same [see Eqs. (7) and (8)] as the requirement that $J = J_c$ or

$$J_\phi(\rho) = J_{c\phi}(\rho) \equiv (J_c^2 - J_\rho^2)^{1/2} = J_c(1 - a^2/\rho^2)^{1/2}, \quad a < \rho < R, \tag{11}$$

where R is the radius of the disk. We shall refer to $J_{c\phi}(\rho)$ as the azimuthal critical current density. The resulting magnetic flux density $\mathbf{B}$ in the presence of the current I can be computed by substituting the current density $J_\phi(\rho)$ from Eqs. (10) and (11) into the Biot-Savart law. In the plane of the film, $B_z(\rho,0)$ can be calculated from Eq. (1). Out of the plane of the film, $B_z(\rho,z)$ and $B_\rho(\rho,z)$ can be calculated from[11]

$$B_z(\rho,z)/B_d = (1/\pi J_c)\int_0^R G_z(\rho,z;\rho') J_\phi(\rho') d\rho', \tag{12}$$

$$B_\rho(\rho,z)/B_d = (1/\pi J_c)\int_0^R G_\rho(\rho,z;\rho') J_\phi(\rho') d\rho', \tag{13}$$

where

$$G_z(\rho,z;\rho')=\frac{1}{\sqrt{(\rho+\rho')^2+z^2}}\left\{K[k(\rho,z;\rho')]-\frac{\rho^2+z^2-\rho'^2}{(\rho-\rho')^2+z^2}E[k(\rho,z;\rho')]\right\}, \quad (14)$$

$$G_\rho(\rho,z;\rho')=\frac{z}{\rho\sqrt{(\rho+\rho')^2+z^2}}\left\{-K[k(\rho,z;\rho')]+\frac{\rho^2+z^2+\rho'^2}{(\rho-\rho')^2+z^2}E[k(\rho,z;\rho')]\right\}, \quad (15)$$

$$k(\rho,z;\rho')=2(\rho'\rho)^{1/2}/\sqrt{(\rho+\rho')^2+z^2}; \quad (16)$$

K and E are complete elliptic integrals with modulus k, as in Eq. (2).

Figure 2(a) shows a sequence of normalized current-density profiles $J_\phi(\rho)/J_c$ for a increasing from zero to $0.5R$. Alternatively, since the relation $B_\rho(\rho,z=0^+)/B_d=J_\phi(\rho)/J_c$ follows from Ampère's law and the symmetry property $B_\rho(\rho,z=0^-)=-B_\rho(\rho,z=0^+)$, we may regard Fig. 2(a) as a sequence of normalized radial magnetic flux density profiles just above the surface. As can be seen from Eq. (9), a can be increased experimentally by increasing the transport current I or increasing the temperature (and thereby decreasing J_c). Figure 2(b) shows the corresponding sequence of normalized flux-density profiles $B_z(\rho,0)$. The flux density at the origin is

$$B_z(0,0)/B_d=\cosh^{-1}(R/a)-(1-a^2/R^2)^{1/2}. \quad (17)$$

Note that all the trapped magnetic flux is expelled when $a=R$.

It is possible that measurements of B_ρ and B_z cannot be made exactly at the top surface of the disk, but that they can be made (perhaps with horizontally and vertically mounted Hall probes) at a finite distance z above the disk's midplane. As an example of how one may analyze the fields in such a case, Figs. 3(a) and 3(b) show profiles of B_ρ and B_z at a height $z=0.1R$, calculated numerically with the help of Eqs. (13) and (12). Although we concentrate in the remainder of this paper on the behavior of the azimuthal current density $J_\phi(\rho)$ and the perpendicular component of the magnetic flux density $B_z(\rho,0)$ in the plane $z=0$, corresponding values of $B_\rho(\rho,z)$ and $B_z(\rho,z)$ at arbitrary heights z always can be obtained from Eqs. (13) and (12), respectively.

The magnetization of the disk is[12]

$$M_z=\int_0^R d\rho(\rho/R)^2J_\phi(\rho), \quad (18)$$

such that for gradually increasing values of a,

$$M_z/M_s=(1-a^2/R^2)^{3/2}, \quad (19)$$

where

$$M_s=J_cR/3 \quad (20)$$

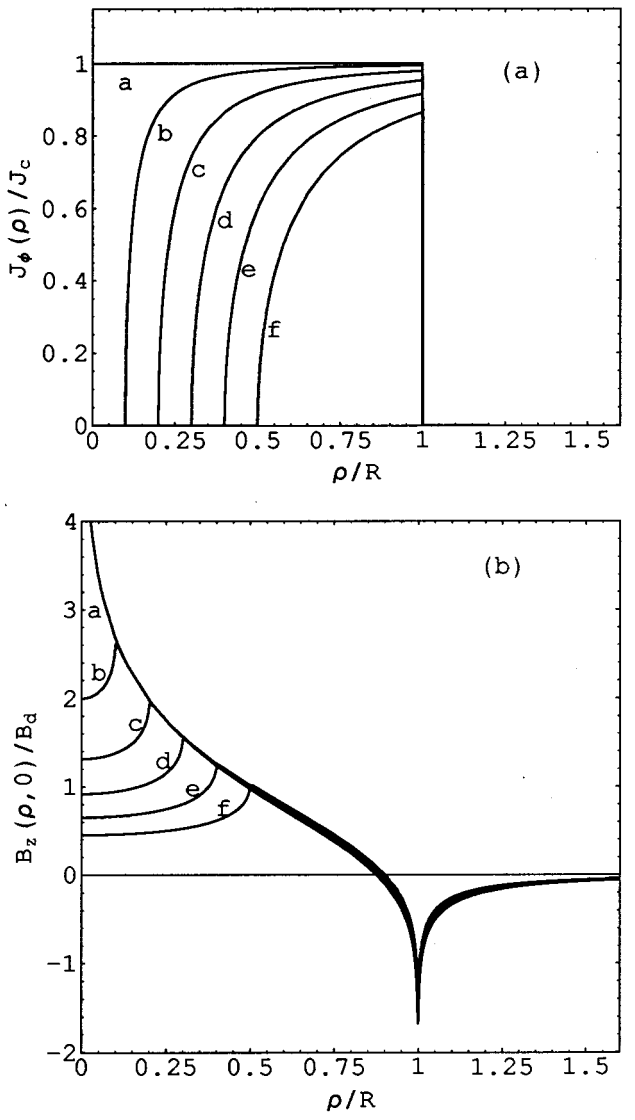

FIG. 2. (a) Azimuthal current density in the remanent state $J_\phi(\rho)$ [Eq. (11)], normalized to the critical current density J_c, vs ρ/R for increasing radial current I, parametrized by $a=I/2\pi J_cd$ [Eq. (9)], for $a/R=$ (a) 0, (b) 0.1, (c) 0.2, (d) 0.3, (e) 0.4, and (f) 0.5. (b) Corresponding remanent-state flux density $B_z(\rho,0)$ in the plane of the Corbino disk, calculated from Eqs. (1) and (11) and normalized to $B_d=\mu_0H_d=\mu_0J_cd/2$, vs ρ/R for the same radial currents I as above.

is the saturation magnetization[9,10,13] corresponding to the result obtained from Eq. (18) when $a=0$ and $J_\phi(\rho)=J_c$. We shall use M_s later in this paper for normalizing the magnetization.

III. BEHAVIOR UPON INITIAL PENETRATION OF MAGNETIC FLUX INTO A CURRENT-CARRYING CORBINO DISK

Consider a thin type-II superconducting disk that has been cooled into the superconducting state in the absence of both a transport current and a perpendicular applied magnetic field. Suppose that a current I is now fed into the sample as

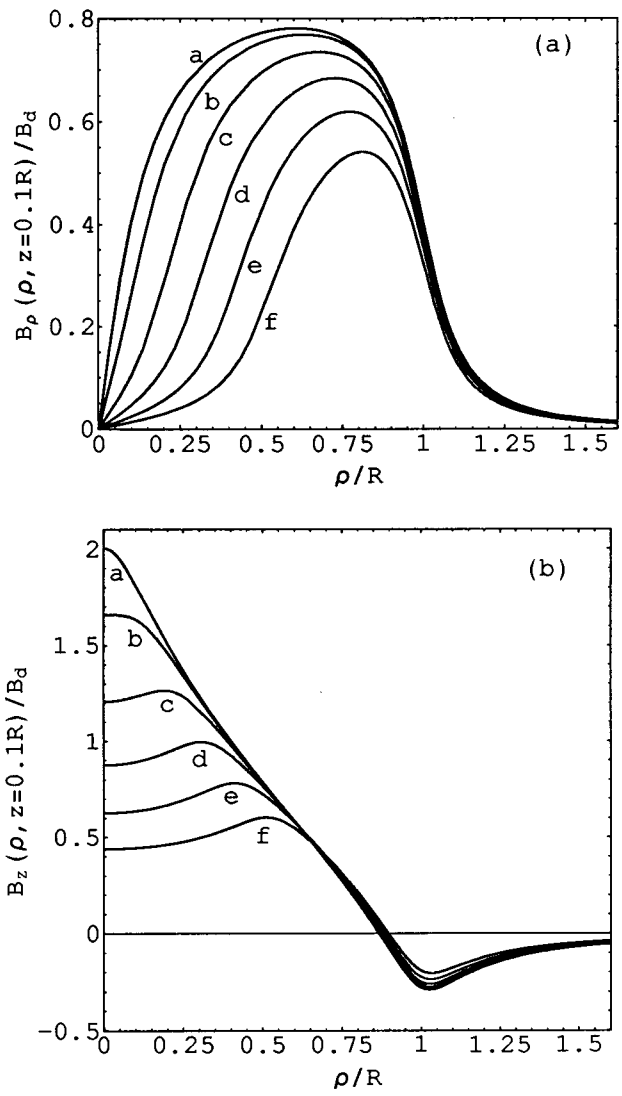

FIG. 3. (a) Radial magnetic-flux density in the remanent state at height $0.1R$ above the disk's surface, $B_\rho(\rho,z=0.1R)$, calculated from Eqs. (11) and (13), and (b) corresponding remanent-state flux density $B_z(\rho,z=0.1R)$, calculated from Eqs. (11) and (12), vs ρ/R for the same radial currents I as in Fig. 2. Both B_ρ and B_z are normalized to $B_d=\mu_0 H_d=\mu_0 J_c d/2$.

shown in Fig. 1. The average radial current density is $J_\rho = I/2\pi\rho d$, where ρ is the radial coordinate and d is the thickness of the disk. We suppose that the self-field at the top surface of the disk, $B_\phi=-\mu_0 I/2\pi\rho$, has magnitude less than $\mu_0 H_{c1}$, such that the superconductor remains in the vortex-free Meissner state; to satisfy this condition, the radius r_c of the central lead and its contact to the disk must obey $r_c > I/2\pi H_{c1}$. We shall see that when a perpendicular magnetic field $\mathbf{B}_a=B_a\hat{z}$ is applied, magnetic flux penetrates into the disk in three stages.

We use the Bean critical-state model, in which the type-II superconductor is characterized by a field-independent critical current density J_c. In the absence of a radial current, the penetration of magnetic flux into the sample, expressed in terms of profiles of the magnetic flux density in the disk $B_z(\rho,0)$ as a function of B_a, can be calculated as in Refs. 9,13 and 10. In the present of a radial current, however, the calculation becomes more difficult because the azimuthal critical current density $J_{c\phi}(\rho)$ [Eq. (11)] depends upon the radial coordinate ρ in that region of the sample where magnetic flux has penetrated. Moreover, the inner regions of the disk where magnetic flux has not yet penetrated [i.e., where $B_z(\rho,0)=0$] carry a Meissner-screening current $J_\phi(\rho)$, which needs to be calculated separately. We assume that in these regions the magnitude of the tangential magnetic field at the top surface remains less than $\mu_0 H_{c1}$, such that they remain in the vortex-free Meissner state. To carry out calculations accounting for the central Meissner-screening regions, we have adapted an approach recently introduced by Shantsev *et al.*[7,8]

An integral-equation method for calculating the penetration of magnetic flux into an infinitely long strip characterized by an arbitrary critical current density $J_c(B)$ was reported by McDonald and Clem in Ref. 14. Shantsev *et al.*[7] found a similar method for calculating the penetration of magnetic flux into a disk characterized by an arbitrary critical current density $J_c(B)$, and in Ref. 8 they applied this method to calculate the magnetization and ac susceptibility for several models for the B dependence of $J_c(B)$. In contrast to the results of Refs. 9,13 and 10, in which the Bean model (J_c independent of B) was assumed, Shantsev *et al.* found suppressed values of J at the edges of the disk, where B is large,[7] and they found that hysteretic magnetization loops narrowed at large values of the applied field.[8] The particular feature of the approach of Shantsev *et al.* that we shall apply in solving the Corbino-disk problem is its ability to account for the dependence of the azimuthal critical current density $J_{c\phi}(\rho)$ upon the radial coordinate ρ.

We assume that for a given applied magnetic field B_a the vortices penetrate from the disk's edge, where strong demagnetizing effects cause the local magnetic field to exceed H_{c1}. We further assume that bulk pinning dominates over edge-pinning effects. The vortices penetrate to the radius b, called the flux-front radius, which initially is a decreasing function of B_a. The local magnetic flux density and the current density are given, respectively, by[7]

$$B_z(\rho,0)=\int_b^{\min(\rho,R)} B_M(\rho,\rho')W(\rho',B_a)d\rho', \qquad (21)$$

$$J_\phi(\rho)=\int_{\max(b,\rho)}^{R} J_M(\rho,\rho')W(\rho',B_a)d\rho', \qquad (22)$$

where $B_M(\rho,\rho')$ is the z component of the Meissner-state flux density vs ρ in the plane of a disk of radius ρ' [$B_M(\rho,\rho')=0$ for $\rho<\rho'$] in an applied field B_a, $J_M(\rho,\rho')$ is the corresponding Meissner-state current density vs ρ,[15,9,13,10] and $W(\rho,B_a)$ is a weight function. Since both $B_z(\rho,0)\to B_a$ and $B_M(\rho,\rho')\to B_a$ at $\rho\to\infty$, we have the normalization condition

$$\int_b^R W(\rho,B_a)d\rho=1. \qquad (23)$$

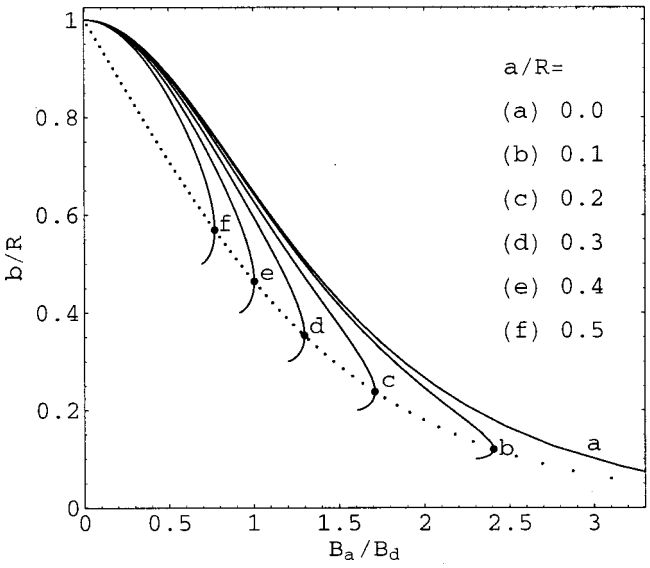

FIG. 4. Flux-front radius b, normalized to the disk radius R, vs applied magnetic induction B_a, calculated from Eq. (25) and normalized to $B_d=\mu_0 H_d=\mu_0 J_c d/2$, for first penetration of magnetic flux and fixed values of $a/R=I/2\pi R J_c d=$ (a) 0, (b) 0.1, (c) 0.2, (d) 0.3, (e) 0.4, and (f) 0.5 (solid curves). Large dots identify values of the maximum applied magnetic induction B_{am} [Eq. (27)] and corresponding flux-front radius b_m [Eq. (28)], where B_{am} is the maximum value of B_a for which magnetic flux penetrates gradually into the sample for a given value of a. The dotted curve shows the trajectory of b_m vs B_{am} [Eq. (29)]. The portions of the solid curves with positive slope (below the large dots and the dotted curve) are unstable, experimentally inaccessible solutions of Eq. (25) for $a<b<b_m$.

From Refs. 7 and 8, we obtain

$$W(\rho,B_a)=-\left(\frac{B_d}{B_a}\right)\frac{d}{d\rho}\int_\rho^R\sqrt{\frac{\rho'^2-a^2}{\rho'^2-\rho^2}}\frac{d\rho'}{\rho'}$$
$$=\left(\frac{B_d}{B_a}\right)\left(\frac{a}{\rho^2}\right)\left[\frac{\rho}{a}\sqrt{\frac{R^2-a^2}{R^2-\rho^2}}-\cosh^{-1}\left(\frac{\rho}{R}\sqrt{\frac{R^2-a^2}{\rho^2-a^2}}\right)\right], \quad (24)$$

where $B_d=\mu_0 J_c d/2$. Substitution of Eq. (24) into Eq. (23) yields an equation determining the flux-front radius b as a function of the applied field B_a:

$$\frac{B_a}{B_d}=\tanh^{-1}\sqrt{\frac{R^2-b^2}{R^2-a^2}}-\frac{a}{b}\tanh^{-1}\left(\frac{a}{b}\sqrt{\frac{R^2-b^2}{R^2-a^2}}\right). \quad (25)$$

In the absence of any transport current ($a=0$), Eq. (25) can be reexpressed as

$$\mathrm{sech}(B_a/B_d)=b/R, \quad (26)$$

which is shown as curve a in Fig. 4. The other solid curves in Fig. 4 show b vs B_a for nonzero transport current I parametrized by $a/R=I/2\pi R J_c d$. Note that for nonzero a, the curves of b vs B_a have infinite slope at the points marked with large dots. In other words, with increasing applied field B_a, the penetration of magnetic flux proceeds by means of a gradually shrinking flux-front radius b only up to a maximum field B_{am}, which depends upon the transport current. By differentiation of Eq. (25), we find for a given a that this maximum field is

$$B_{am}/B_d=\tanh^{-1}[1+(\beta^2-1)(a/R)^2]^{-1/2}-[1+(\beta^2-1)(a/R)^2]^{1/2}, \quad (27)$$

where $\beta=1.199\,679$ is the solution of $\beta\tanh\beta=1$. The corresponding flux-front radius is

$$b_m=\beta a[1+(\beta^2-1)(a/R)^2]^{-1/2}. \quad (28)$$

The dotted curve connecting the large dots in Fig. 4 (B_{am} vs b_m) is obtained by eliminating a between Eqs. (27) and (28):

$$B_{am}/B_d=\tanh^{-1}[1-(1-\beta^{-2})(b_m/R)^2]^{1/2}-[1-(1-\beta^{-2})(b_m/R)^2]^{-1/2}. \quad (29)$$

The portions of the curves of b vs B_a with positive slope in Fig. 4 for $a<b<b_m$ are unstable, experimentally inaccessible solutions of Eq. (25).

During the initial penetration of magnetic flux into the Corbino disk in the presence of a radial transport current I and an applied magnetic field B_a, the normalized magnetic flux density $B_z(\rho,0;b)/B_d$ in the plane of the disk ($z=0$) and the normalized azimuthal current density $J_\phi(\rho;b)/J_c$ are as follows:[7,8]

$$B_z(\rho,0;b)/B_d=B_a/B_d+(1/\pi J_c)\int_0^R G(\rho,\rho')J_\phi(\rho';b)d\rho', \quad (30)$$

$$\frac{J_\phi(\rho;b)}{J_c}=-\frac{2}{\pi}\int_b^R\frac{\rho\sqrt{b^2-\rho^2}}{\rho'(\rho'^2-\rho^2)}\sqrt{\frac{\rho'^2-a^2}{\rho'^2-b^2}}d\rho', \quad \rho<b, \quad (31)$$

$$=-\sqrt{1-a^2/\rho^2}, \quad b<\rho<R, \quad (32)$$

where $G(\rho,\rho')$ is defined in Eq. (2).

Although $B_z(\rho,0;b)$ has to be evaluated numerically from Eq. (30), $J_\phi(\rho;b)$ can be obtained analytically from Eqs. (31) and (32):

$$\frac{J_\phi(\rho;b)}{J_c} = -\frac{2}{\pi\rho}\left[\frac{a}{b}\sqrt{b^2-\rho^2}\tanh^{-1}\left(\frac{a}{b}\sqrt{\frac{R^2-b^2}{R^2-a^2}}\right) - \sqrt{a^2-\rho^2}\tanh^{-1}\sqrt{\frac{(R^2-b^2)(a^2-\rho^2)}{(R^2-a^2)(b^2-\rho^2)}}\right] \quad (0\leqslant\rho\leqslant a\leqslant b), \tag{33}$$

$$= -\frac{2}{\pi\rho}\left[\frac{a}{b}\sqrt{b^2-\rho^2}\tanh^{-1}\left(\frac{a}{b}\sqrt{\frac{R^2-b^2}{R^2-a^2}}\right) + \sqrt{\rho^2-a^2}\tan^{-1}\sqrt{\frac{(R^2-b^2)(\rho^2-a^2)}{(R^2-a^2)(b^2-\rho^2)}}\right] \quad (a\leqslant\rho\leqslant b) \tag{34}$$

$$= -\frac{\sqrt{\rho^2-a^2}}{\rho} \quad (b\leqslant\rho\leqslant R). \tag{35}$$

Shown in Fig. 5(a) is a plot of $|J_\phi(\rho;b)|/J_c$ [Eqs. (33), (34), and (35)] vs ρ/R for fixed $a/R=0.2$ and a sequence of increasing applied fields B_a [Eq. (25)] and decreasing flux-front radii b: $(B_a/B_d, b/R)=$ (a) (0.674, 0.800), (b) (1.053, 0.600), (c) (1.446, 0.400), and (d) $(B_{am}/B_d, b_m/R)$ $=$(1.710, 0.238). Figure 5(b) shows a plot of the corresponding flux-density profiles $B_z(\rho,0;b)/B_d$ vs ρ/R, calculated numerically by combining Eqs. (30), (33), (34), and (35). A comparison of Fig. 5(a) with Figs. 3 and 4 of Shantsev *et al.*,[7] who account for the B dependence of J_c, reveals some important differences. In the present treatment, based upon the Bean model (J_c independent of B), the radial transport current suppresses the azimuthal current density [see Eq. (11)] near the center of the disk, where the radial current density is largest. Shantsev *et al.*,[7] in examining cases for which $J_c(B)$ is a decreasing function of B, found that the azimuthal current density is enhanced at the flux front, where B is small, and suppressed near the edge of the disk, where B is large.

From Fig. 4 we have seen that for fixed current I (fixed a) and increasing applied field B_a, the initial penetration of magnetic flux into a current-carrying Corbino disk begins with a gradually shrinking flux-front radius b. Typical current-density and flux-density profiles were shown in Figs. 5(a) and 5(b). Vortices are present in the region $b<\rho<R$, where the magnitude of the azimuthal current density $J_\phi(\rho)$ is equal to the effective azimuthal critical current density $J_{c\phi}(\rho)=J_c(1-a^2/\rho^2)^{1/2}$. No vortices are present in the region $\rho<b$, which remains in the Meissner state and is thus capable of supporting a large screening supercurrent, given in Eqs. (33) and (34). This *first stage* of flux penetration ends when B_a grows to the value B_{am} [Eq. (27)] and b shrinks to the value b_m [Eq. (28)]. We now address the question of what happens during the second stage of flux penetration, which begins at $B_a=B_{am}$.

Note from curves $a-c$ of Fig. 5(a) that the magnitude of the screening current density $J_\phi(\rho)$ drops rapidly below $J_{c\phi}(\rho)$ for $\rho<b$ throughout the first stage of flux penetration. This means that vortices at the flux-front radius b are stable when $B_a<B_{am}$; i.e., any vortex with radial coordinate ρ slightly less than b remains pinned. However, as shown by curve d in Fig. 5(a) and the dashed curve showing $J_{c\phi}(\rho)$, when $B_a=B_{am}$, the curve of $J_\phi(\rho)$ vs ρ becomes tangent to $J_{c\phi}(\rho)$ at $\rho=b_m$. A vortex with radial coordinate ρ slightly less than b_m thus experiences an azimuthal current density $J_\phi(\rho)$ of magnitude greater than $J_{c\phi}(\rho)$. Since this leads to an inward Lorentz force exceeding the pinning force, such a vortex will be driven inward towards the center of the disk.

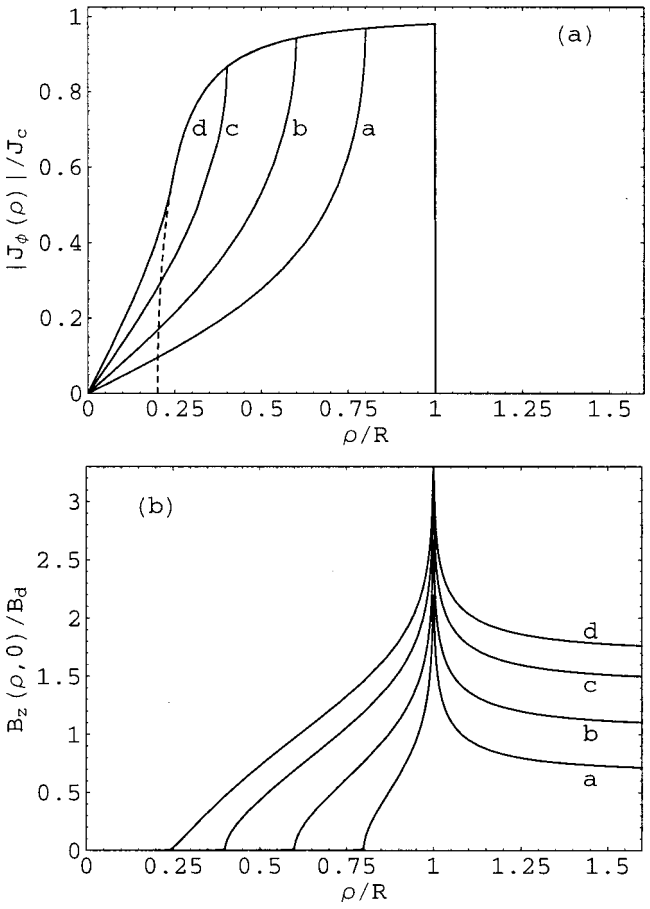

FIG. 5. (a) Magnitude of the azimuthal current density $|J_\phi(\rho;b)|$, normalized to J_c, vs ρ/R during the first stage of flux penetration for $a/R=0.2$ and a sequence of increasing applied fields B_a and decreasing flux-front radii b [Eq. (25)]: $(B_a/B_d, b/R)=$ (a) (0.674, 0.800), (b) (1.053, 0.600), (c) (1.446, 0.400), and (d) $(B_{am}/B_d, b_m/R)=$ (1.710, 0.238). (b) Corresponding flux-density profiles $B_z(\rho,0;b)/B_d$ vs ρ/R, calculated from Eq. (30).

From this we see that the *second stage* of flux penetration, characterized by the sudden inflow of a finite amount of magnetic flux, is triggered by an instability that occurs when $B_a=B_{am}$. When the applied field B_a slightly exceeds B_{am}, vortices are pushed inside the critical flux-front radius b_m, and the azimuthal current density J_ϕ, since it exceeds the azimuthal critical current density $J_{c\phi}(\rho)$, drives the vortices towards the center of the disk. This generates a negative azumuthal component of the electric field, $E_\phi(\rho)$, which, according to Faraday's law, is accompanied by an increase in

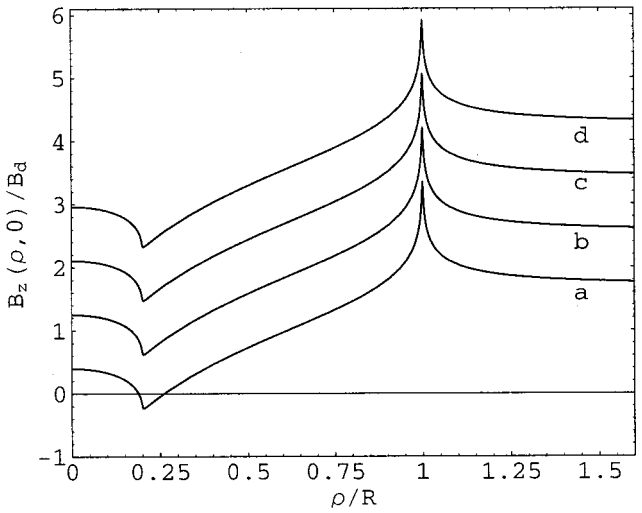

FIG. 6. Flux-density profiles $B_z(\rho,0)/B_d$ vs ρ/R during the third stage of flux penetration, calculated from Eq. (30) for $a/R=0.2$ but with J_ϕ taken from Eqs. (36) and (37) for increasing applied magnetic induction $B_a=$ (a) B_{am}, (b) 1.5 B_{am}, (c) 2.0 B_{am}, and (d) 2.5 B_{am}, where $B_{am}=1.710B_d$.

the z component of the magnetic flux in the interior of the disk. The rapid, inward flow of vortices is initially uncontrolled except via viscous drag forces and the corresponding flux-flow resistivity. As more and more vortices fill the middle of the disk, the region $0<\rho<a$ becomes resistive; a radial electric field E_ρ is now generated, because vortices with $0<\rho<a$ experience a radial current density J_ρ greater than J_c; these vortices eventually take up circular trajectories around the axis of the disk. Vortices continue to flow into the central portion of the disk and to redistribute finally in such a way that the second stage of flux penetration is concluded when the azimuthal current density J_ϕ takes on the final distribution,

$$J_\phi(\rho)=0, \quad 0<\rho<a, \tag{36}$$

$$J_\phi(\rho)=-J_{c\phi}(\rho)=-J_c(1-a^2/\rho^2)^{1/2}, \quad a<\rho<R. \tag{37}$$

The z and ρ components of the resulting magnetic field now can be calculated as the superposition of (a) the uniform applied magnetic field B_a in the z direction and (b) the magnetic field calculated via the Biot-Savart law [Eqs. (12) and (13)] from the azimuthal current density $J_\rho(\rho)=-J_{c\phi}(\rho)$ in the region $a<\rho<R$. There is a significant change in the magnetic flux distribution $B_z(\rho,0)$ and a large increase of magnetic flux inside the radius b_m resulting from this second-stage flux entry. This can be seen by comparing curve d in Fig. 5(b) at the end of stage one with curve a in Fig. 6, which represents $B_z(\rho,0)$ vs ρ at the end of stage 2 and the beginning of stage 3. At the end of the second stage of flux penetration, there remains a nonzero steady-state radial electric field E_ρ for $\rho<a$, where vortices are continuously driven around the disk's axis in circular trajectories, and $E_\rho=0$ for $\rho>a$, where vortices are now pinned in the critical state. The azimuthal component of the electric field, E_ϕ, vanishes.

A *third stage* of flux penetration occurs as the applied field B_a is gradually increased above B_{am}. Vortices are nucleated at the outer radius of the sample and driven inward by the induced azimuthal current density, whose magnitude is just above $J_{c\phi}(\rho)$. At each value of B_a, the magnetic flux density can be calculated as the superposition of the uniform applied magnetic field and the field generated by the azimuthal current density in the region $a<\rho<R$. A sequence of profiles of $B_z(\rho,0)$ vs ρ for increasing values of B_a is shown in Fig. 6. As at the end of stage two, the sample interior is resistive; i.e., there is a steady-state radial electric field E_ρ in the region $\rho<a$, where the radial current density J_ρ exceeds J_c.

The magnetic moment of a disk carrying a current with only an azimuthal current density J_ϕ has only a z component,

$$m_z=\frac{1}{2}\int \rho J_\phi d^3\rho. \tag{38}$$

We define the corresponding magnetization as $M_z=m_z/V$, where $V=\pi R^2 d$ is the sample volume. We wish to calculate the initial magnetization when a superconducting Corbino disk in the Meissner state is carrying a radial current I and a perpendicular magnetic field $\mathbf{B}_a=B_a\hat{z}$ is applied, as above. Substitution of Eqs. (33), (34), and (35) into Eq. (38) yields the initial magnetization, normalized to the saturation magnetization $M_s=RJ_c/3$ for $a=0$:

$$\frac{M_z}{M_s}=-\frac{2}{\pi R^3}\left[a(b^2-a^2)\tanh^{-1}\left(\frac{a}{b}\sqrt{\frac{R^2-b^2}{R^2-a^2}}\right)\right.$$
$$\left.+(R^2-a^2)^{3/2}\cos^{-1}(b/R)+b\sqrt{(R^2-a^2)(R^2-b^2)}\right]$$
$$\equiv M_{zi}(a,b)/M_s \tag{39}$$

Equation (39) yields the initial magnetization M_z as a function of the flux-front radius b for fixed current I (fixed a). To obtain M_z vs the applied field B_a, one needs only to make use of Eq. (25), which can be solved to obtain b as a function of B_a. It can be shown that when there is no radial current I ($a=0$), the magnetization reduces to the results given in Refs. 9,10, and 13. It also can be shown that the slope of the initial magnetization at $B_a=0$ is independent of a and behaves as

$$\frac{M_z}{M_s}=-\frac{4}{\pi}\frac{B_a}{B_d}, \quad \frac{B_a}{B_d}\ll 1, \tag{40}$$

the same as the behavior of a disk with perfect screening.[10]

Equation (39) holds only for the first stage of initial flux penetration, i.e., only for $b_m<b<R$ and $0<B_a<B_{am}$. The sudden entry of magnetic flux that occurs during the second stage of flux penetration when $b=b_m$ and $B_a=B_{am}$ leads to a jump in the magnetization. During the third stage of flux penetration, the current density is given by Eqs. (36) and (37), and the corresponding normalized magnetization obtained from Eq. (18) or Eq. (38) is

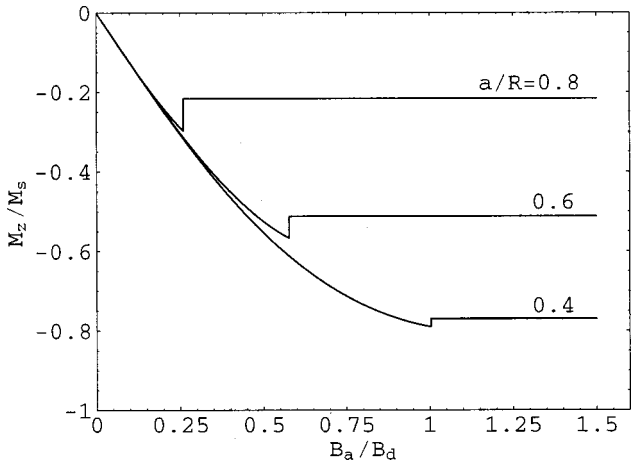

FIG. 7. Magnetization M_z, normalized to $M_s = J_c R/3$, vs increasing applied magnetic induction B_a, normalized to $B_d = \mu_0 H_d = \mu_0 J_c d/2$, for initial penetration of magnetic flux into the Corbino disk for three different radial currents I, corresponding to $a/R = 0.4$, 0.6, and 0.8, calculated from Eqs. (39) and (41).

$$M_z/M_s = -(1-a^2/R^2)^{3/2}, \tag{41}$$

the negative of that given in Eq. (19).

Shown in Fig. 7 are plots of the magnetization M_z (normalized to M_s) vs applied field B_a (normalized to B_d) for the initial penetration of magnetic flux into a current-carrying Corbino disk for several values of a. Note the jumps in magnetization occurring at B_{am}. Increasing the radial current I (i.e., increasing a) decreases the magnitude of M_z, which is always less than M_s.

IV. ac PROPERTIES

We next calculate the current-density and flux-density profiles produced when a perpendicular applied field oscillates between $+h_0$ and $-h_0$, restricting our attention to stage-1 flux penetration, in which disk's center remains in the Meissner state. We begin with the profiles for which the applied magnetic induction along the $+z$ direction has increased monotonically from zero to $B_a = +b_0 = +\mu_0 h_0$. The corresponding initial flux-front radius b can be obtained, as in Sec. III, by solving Eq. (25) with $B_a = b_0$. We next investigate what happens when the applied magnetic induction is monotonically decreased from $+b_0$ to a value in the range $-b_0 \leqslant B_a \leqslant +b_0$. We may calculate the resulting current density using the procedure explained in Refs. 13 and 10. When $B_a = +b_0$, the azimuthal current density is $J_\phi = -J_c\sqrt{1-a^2/\rho^2}$ in the region $b \leqslant \rho \leqslant R$, as in Eq. (35). However, as B_a decreases, the current density changes sign and takes on the value $J_\phi = +J_c\sqrt{1-a^2/\rho^2}$ in the annular region $c \leqslant \rho \leqslant R$, where $b \leqslant c \leqslant R$. As B_a decreases, the magnetic-flux density $B_z(\rho,0)$ remains unchanged throughout the region $0 \leqslant \rho \leqslant c$. Using an argument similar to that used in Refs. 13 and 10, we find that the current density while B_a is decreasing is

$$J_\phi(\rho;b,c) = J_\phi(\rho;b) - 2J_\phi(\rho;c), \tag{42}$$

where the function $J_\phi(\rho;b)$ is defined in Eqs. (33), (34), and (35), and the ac penetration radius c remains to be determined. The corresponding magnetic flux density in the plane of the disk is found to be

$$B_z(\rho,0;b,c) = B_z(\rho,0;b) - 2B_z(\rho,0;c), \tag{43}$$

where the terms on the right-hand side of this equation are calculated from Eq. (30) with the help of Eqs. (33), (34), and (35).

The inner radius c of the annular region in which $J_\phi = +J_c\sqrt{1-a^2/\rho^2}$, together with the results given in Eqs. (42) and (43), is obtained with the help of a weight function, which can be derived by a method similar to that used in Sec. III:

$$\frac{b_0 - B_a}{2B_d} = \tanh^{-1}\sqrt{\frac{R^2-c^2}{R^2-a^2}} - \frac{a}{c}\tanh^{-1}\left(\frac{a}{c}\sqrt{\frac{R^2-c^2}{R^2-a^2}}\right). \tag{44}$$

Note that Eq. (44) could have been obtained from Eq. (25) simply by replacing B_a by $b_0 - B_a$, B_d by $2B_d$, and b by c. Note also from Eqs. (44) and (25) that $c = R$ when $B_a = b_0$ and $c = b$ when $B_a = -b_0$.

Shown in Fig. 8 are profiles of (a) the azimuthal current density $J_\phi(\rho)$ [Eqs. (42), (33), (34), (35), (25), and (44)] and (b) the magnetic flux density $B_z(\rho,0)$ [Eq. (43)] vs ρ under ac conditions for the field-decreasing half cycle as the applied magnetic induction B_a decreases from $+b_0 = 1.5B_d$ to $-b_0 = -1.5B_d$ for radial current I corresponding to $a/R = 0.2$.

For the field-increasing half cycle (B_a increasing from $-b_0$ to $+b_0$), it is straightforward to show that

$$J_\phi(\rho;b,c') = -J_\phi(\rho;b) + 2J_\phi(\rho;c'), \tag{45}$$

where $J_\phi(\rho;b)$ is given by Eqs. (33), (34), (35), and (25) with $B_a = +b_0$. Following a derivation similar to that leading to Eq. (44), we find that c' is determined from

$$\frac{b_0 + B_a}{2B_d} = \tanh^{-1}\sqrt{\frac{R^2-c'^2}{R^2-a^2}} - \frac{a}{c'}\tanh^{-1}\left(\frac{a}{c'}\sqrt{\frac{R^2-c'^2}{R^2-a^2}}\right). \tag{46}$$

For B_a increasing, $c' = R$ when $B_a = -b_0$, and $c' = b$ when $B_a = +b_0$. The corresponding magnetic flux density in the plane of the disk is found to be

$$B_z(\rho,0;b,c') = -B_z(\rho,0;b) + 2B_z(\rho,0;c'), \tag{47}$$

where the terms on the right-hand side of this equation are calculated from Eq. (30) with the help of Eqs. (33), (34), and (35).

We next show how to calculate the hysteretic magnetization of a current-carrying Corbino disk subjected to a perpendicular ac applied magnetic field, again restricting our attention to stage-1 flux penetration, in which disk's center remains in the Meissner state. Here, since the external magnetic field is applied along the $+z$ direction, the magnetic moment has only a z component, given by Eq. (38). In Sec. III, we considered a current-carrying Corbino disk in the

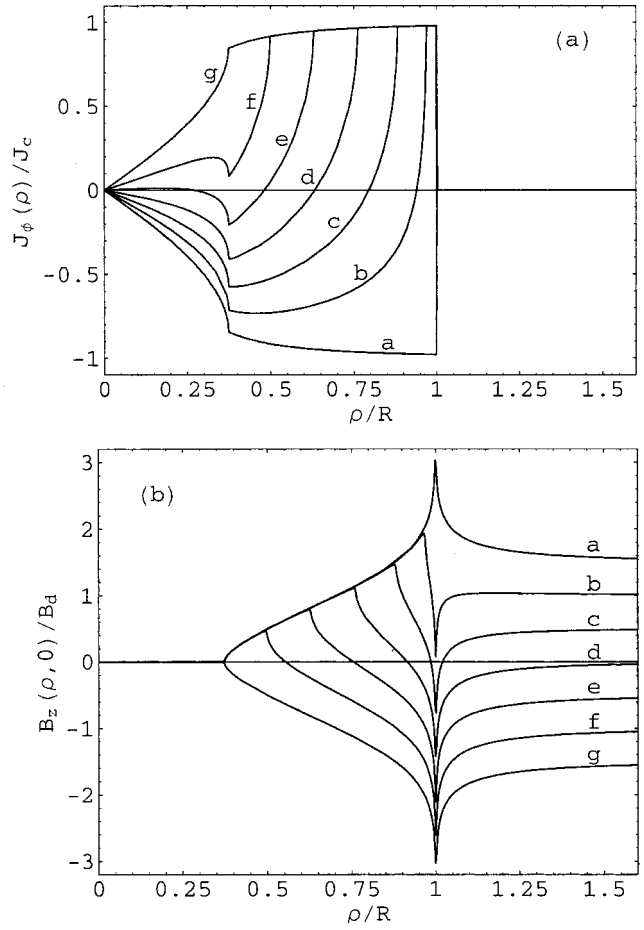

FIG. 8. (a) Profiles of the current density $J_\phi(\rho)$, normalized to the critical current density J_c, vs the reduced radial coordinate ρ/R for a Corbino disk of radius R carrying a radial transport current I, parametrized by $a/R=I/2\pi RJ_cd=0.2$, as the normalized applied ac magnetic field B_a/B_d is decreased from $b_0/B_d=+1.5$ to $-b_0/B_d=-1.5$: $B_a/B_d=$ (a) 1.5, (b) 1.0, (c) 0.5, (d) 0.0, (e) -0.5, (f) -1.0, and (g) -1.5. The azimuthal current densities are calculated from Eq. (42), and the flux-front radius b and ac penetration radius c are given by Eqs. (25) and (44), respectively. (b) Corresponding flux-density profiles $B_z(\rho,0)/B_d$, calculated from Eq. (43).

Meissner state and calculated its initial magnetization, which we denoted by $M_{zi}(a,b)$ [Eq. (39)]. Suppose that the applied magnetic induction B_a has been increased to the value $+b_0$ and is now decreased from $+b_0$ to $-b_0$. We may use the results of Sec. III to obtain the decreasing-field magnetization, denoted by $M_{z\downarrow}(a,b,c)$, by substituting Eq. (42) into Eq. (38) and carrying out a calculation similar to that used in deriving Eq. (39). The resulting normalized field-decreasing magnetization $M_{z\downarrow}$ is

$$M_{z\downarrow}(a,b,c)/M_s=M_{zi}(a,b)/M_s-2M_{zi}(a,c)/M_s, \tag{48}$$

where the normalized initial magnetization $M_{zi}(a,b)/M_s$ is given by Eq. (39), a is given by Eq. (9), b is given by Eq. (25) with $B_a=+b_0$, and c is given by Eq. (44).

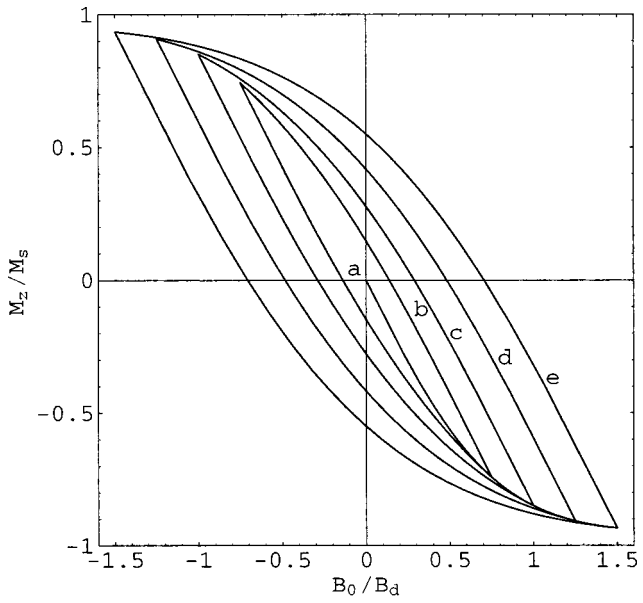

FIG. 9. Normalized magnetization M_z/M_s vs reduced applied magnetic field B_a/B_d for a superconducting Corbino disk carrying radial current I parametrized by $a/R=I/2\pi RJ_cd=0.2$. Curve a shows the initial magnetization [Eq. (39)], starting from the zero-field-cooled state. The remaining curves show magnetization hysteresis loops [Eqs. (48) and (49)] when $B_a=\mu_0H_a$ is cycled between $+b_0$ and $-b_0$ for $b_0/B_d=$ (b) 0.75, (c) 1.00, (d) 1.25, and (e) 1.50.

Similarly, when the applied magnetic induction is increased from $-b_0$ to $+b_0$, the reduced increasing-field magnetization $M_{z\uparrow}$ is

$$M_{z\uparrow}(a,b,c')/M_s=-M_{zi}(a,b)/M_s+2M_{zi}(a,c')/M_s, \tag{49}$$

where c' is given by Eq. (46).

Figure 9 shows plots of the magnetization hysteresis loops calculated from Eqs. (48) and (49) for four values of $b_0=\mu_0h_0$ but the same value of the transport current parametrized by $a/R=I/2\pi RJ_cd=0.2$. The curve beginning at the origin is the initial magnetization, Eq. (39).

V. SUMMARY

In this paper, we have used the critical-state model to analyze the magnetization of a thin, superconducting current-carrying Corbino disk of radius R and thickness d subjected to a perpendicular magnetic field. We first considered, in Sec. II, a disk carrying no radial current but containing remanent magnetic flux in zero applied magnetic field. We found that when a radial current I is then applied to the Corbino disk, the disk's central region (radius $a=I/2\pi J_cd$) becomes resistive, rendering it unable to sustain azimuthal persistent currents there, such that some of the trapped flux is expelled. When the radial current density reaches J_c at the outer radius R of the disk, all the trapped flux is expelled.

We next considered, in Sec. III, a disk initially in the Meissner state and carrying a radial current, but containing no trapped magnetic flux in zero applied magnetic field. To

calculate the profiles of the azimuthal current density and the perpendicular component of the magnetic-flux density when a perpendicular magnetic field is first applied, we applied a method first introduced by Shantsev *et al.*[7,8] for another purpose. We found that magnetic-flux penetration into the disk occurs in three stages. In the first stage, magnetic flux gradually penetrates up to a flux-front radius b, while the disk's interior ($\rho<b$) remains in the Meissner state. In the second stage, initiated by an instability, magnetic flux suddenly rushes into the disk's interior, making the central region of the disk ($\rho<a$) resistive and unable to carry persistent azimuthal currents. In the third stage, the magnetic flux distribution is describable as the sum of the externally applied magnetic induction B_a and the Biot-Savart-derived magnetic field generated by an azimuthal critical current density flowing in an annulus of inner radius a and outer radius R. Using the analytic results obtained in this section, we then calculated the initial magnetization of the disk.

In Sec. IV, we calculated sequences of profiles of the azimuthal current density and the perpendicular component of the magnetic-flux density when a perpendicular ac magnetic field is applied to a current-carrying Corbino disk initially in the Meissner state. We restricted our attention to field amplitudes corresponding to the first stage of flux penetration, such that the disk's interior remains in the Meissner state. Using the analytic results from this section, we then calculated magnetization hysteresis loops for the Corbino disk.

We hope that this paper will stimulate experimental investigations of the phenomena predicted here.

ACKNOWLEDGMENTS

We are grateful to J. Jung for suggesting this problem, and we thank V. G. Kogan, Y. Mawatari, and A. Gurevich for helpful comments. A.A.B.B. acknowledges sabbatical-leave support from the Isfahan University of Technology. Ames Laboratory is operated for the U.S. Department of Energy by Iowa State University under Contract No. W-7405-Eng-82. This research was supported by the Director for Energy Research, Office of Basic Energy Sciences.

[1] D. Lopez, W. K. Kwok, H. Safar, R. J. Olsson, A. M. Petrean, L. Paulius, and G. W. Crabtree, Phys. Rev. Lett. **82**, 1277 (1999).

[2] D. Lopez, W. K. Kwok, and G. W. Crabtree, Adv. Supercond., 1983 **11**, 565 (1999).

[3] S. F. W. R. Rycroft, R. A. Doyle, D. T. Fuchs, E. Zeldov, R. J. Drost, P. H. Kes, T. Tamegai, S. Ooi, and D. T. Foord, Phys. Rev. B **60**, R757 (1999).

[4] S. F. W. R. Rycroft, R. A. Doyle, D. T. Fuchs, E. Zeldov, R. J. Drost, P. H. Kes, T. Tamegai, S. Ooi, A. M. Campbell, W. Y. Liang, and D. T. Foord, Supercond. Sci. Technol. **12**, 1067 (1999).

[5] Yu. Eltsev, K. Nakao, S. Shibata, and N. Koshizuka, Physica C **341-348**, 1107 (2000).

[6] Y. Paltiel, E. Zeldov, Y. Myasoedov, M. L. Rappaport, G. Jung, S. Bhattacharya, M. J. Higgins, Z. L. Xiao, E. Y. Andrei, P. L. Gammel, and D. J. Bishop, Phys. Rev. Lett. **85**, 3712 (2000).

[7] D. V. Shantsev, Y. M. Galperin, and T. H. Johansen, Phys. Rev. B **60**, 13 112 (1999).

[8] D. V. Shantsev, Y. M. Galperin, and T. H. Johansen, Phys. Rev. B **61**, 9699 (2000).

[9] P. N. Mikheenko and Y. E. Kuzovlev, Physica C **204**, 229 (1993).

[10] J. R. Clem and A. Sanchez, Phys. Rev. B **50**, 9355 (1994).

[11] L. D. Landau and E. M. Lifshitz, *Electrodynamics of Continuous Media* (Addison-Wesley, Reading, MA, 1960).

[12] J. D. Jackson, *Classical Electrodynamics* (Wiley, New York, 1962).

[13] J. Zhu, J. Mester, J. Lockhart, and J. Turneaure, Physica C **212**, 216 (1993).

[14] J. McDonald and J. R. Clem, Phys. Rev. B **53**, 8643 (1996).

[15] M. B. Ketchen, W. J. Gallagher, A. W. Kleinsasser, S. Murphy, and J. R. Clem, in *SQUID'85, Superconducting Quantum Interference Devices and Their Applications*, edited by H. D. Hahlbohm and H. Lübbig (de Gruyter, Berlin, 1985), p. 865.